Characterizing the seismic response and basin structure of Cusco (Peru): implications for the seismic hazard assessment of a World Heritage Site

A. Combey, Diego Enrique Mercerat, Jonathan E. Díaz, Carlos L. Benavente Escóbar, Fredy P. Perez, Briant García, Anderson R. Palomino, César J. Guevara Pillaca

Natural Hazards (10.1007/s11069-024-06912-7)

Characterizing the seismic response and basin structure of Cusco (Peru). Implications for the seismic hazard assessment of a World Heritage Site.

A. Combey[1]*, E.D. Mercerat[1], J.E. Díaz[2], C.L. Benavente[2], F.P. Perez[2], B. García[2], A.R. Palomino[2] and C.J. Guevara[2]

[1] *Université Côte d'Azur, CNRS, Observatoire de la Côte d'Azur, IRD, Géoazur, Sophia Antipolis, 250 Rue Albert Einstein, 06560 Valbonne, France*
[2] *Instituto Geológico Minero y Metalúrgico (INGEMMET), Av. Canadá 1470, San Borja, 15034, Lima, Perú*

*Corresponding author: *andy.combey@geoazur.unice.fr*

Abstract

Known worldwide for its rich and well-preserved pre-Columbian and Spanish architecture, the city of Cusco (Peru) is listed as a World Heritage Site since 1983. However, less well known is the seismic hazard, which represents a major threat to the city's 400,000 inhabitants and its cultural outreach. Despite the moderate magnitudes recorded in the area, macroseismic data inferred from historical earthquakes (1650, 1950) argues for strong amplification effects of the unconsolidated sediments of the Cusco Basin during ground motion. In order to address this aggravating factor for the first time, we conducted a large-scale passive geophysical survey in the historical city center of Cusco, combining Microtremor Horizontal-to-Vertical Spectral Ratio (MHVSR) measurements and Microtremor Array Measurements (MAM). Through joint data inversion, we proposed a subsurface wave velocity model and estimated the depth of the engineering bedrock. The site response analysis not only provides an insight into the thickness of the soft sediment, but also suggests the existence of a strong geological discontinuity beneath the city center of Cusco, consistent with the trace of the Cusco fault. Moreover, the results highlight the complexity of earthquake site amplification assessment in dense urban areas. Our work paves the way for a comprehensive seismic microzonation of the entire Cusco Basin and opens up new perspectives on the potential of the MHVSR method for fault detection.

Keywords: Horizontal-to-Vertical Spectral Ratio (HVSR); site effects; sedimentary basin; Cusco fault; heritage preservation; seismic hazard assessment

1. Introduction

Major earthquake disasters such as those of Mexico City (1985), Kobe (1995) and more recently Turkey-Syria (2023) have demonstrated the increase in hazard caused by the amplification of seismic waves in soft soils, such as alluvial deposits (e.g., Kramer 1996). However, this topic remains in its infancy in the Andes, limited almost exclusively to the capital cities (Santiago: Pilz et al. 2009; Pastén et al. 2015; Lima: Calderon et al. 2014; Quito: Pacheco et al. 2022). As a fast-growing touristic town with uncontrolled planning, the city of Cusco turns out to be a crucial case study. The city, located at an altitude of 3,400 meters on the boundary between the Eastern Cordillera and the Altiplano, is settled in a Quaternary sedimentary basin bordered to the north and south by numerous active faults belonging to the Cusco-Vilcanota fault system (CVFS; Cabrera et al. 1991). Although the seismic hazard in the region is considered moderate – compared with Peru's Pacific margin – the city of Cusco has suffered greatly from the regional seismic activity before the instrumental era. The 1650 ($Mw>6$; Silgado 1978; Combey et al. 2022) and 1950 earthquakes ($5.6<Mw<5.9$; Ericksen et al. 1954; Combey et al. 2022) devastated Cusco, causing extensive damage to many historical buildings. In addition to these disasters, the city's history has been punctuated by other violent tremors, notably in 1744 (Seiner 2016), 1941 (Silgado et al. 1952), 1986 (Cabrera and Sébrier 1998) and 2018 (https://cnnespanol.cnn.com/2018/11/11/sismo-peru-cusco-pisac-magnitud-temblor/ Accessed on 21/07/24).

Although data on Cusco's historical seismicity remains scanty and incomplete (Combey et al. 2022), macroseismic data inferred from the 1650 and 1950 earthquakes advocates for a significant role of local site conditions and site effects in the distribution and extent of damage. Unfortunately, we have little information on the characteristics of the Cusco subsurface geology, especially on its north-western edge, where the historical center is located. No boreholes have ever been drilled in the basin, and the use of this method now seems to be hampered by the dense urbanization of the entire valley. While the city still only occupied the north-western edge of the basin at the beginning of the 20th century, it has undergone rapid and uncontrolled demographic expansion since the 1950s (Fig.1). The population living in the Cusco Basin has more than tripled since 1972, and now accounts for more than 400,000 inhabitants (Census INEI 2017: https://censos2017.inei.gob.pe/redatam/ Accessed on 21/07/24). The existing geotechnical data does not allow for a proper understanding of the geo-structural settings of the basin as well as its potential for dynamic amplification in case of an earthquake. At this stage, the published data only provides information on the surface sediments

(first few meters) and an approximate depth of the basin in its central part (INDECI-PNUD 2003; Barrientos 2021). No extensive geophysical survey has yet been carried out in the historical city center. Hence, there is an urgent need to characterize the physical properties and response of Cusco's subsurface geology in order to better assess the hazard and risk in the event of strong ground shaking. Non-invasive passive geophysical methods such as Microtremor Array Measurements (MAM) and single-station microtremor Horizontal-to-Vertical Spectral Ratio (MHVSR) are particularly suitable for urban environments because they are quick and easy to deploy. Particularly effective in estimating subsoil S-wave velocity structure and mapping soil/rock interface, these methods constitute thus the first step towards a comprehensive seismic microzonation and the identification of potential soil-structure interactions. Listed as a World Heritage site by UNESCO since 1983 for the integrity and authenticity of its architectural heritage, the historical City Center of Cusco (CCC) has a rich Inca and colonial built heritage whose exposure and vulnerability to earthquakes urgently needs to be assessed (Brando et al. 2019).

That is why we carried out a large-scale passive seismic survey in the old city center, combining multichannel and single-station geophysical measurements. Through the joint inversion of both ambient vibration signals, this work aimed to characterize the sediment thickness and their seismic response. To that end, we first outline the geological setting of the Cusco Basin. We then present the different geophysical methods used as part of the seismic surveys. Next, we describe the main results of the microtremor analysis and inversion for estimating bedrock depth. In the Discussion section, we first address the spatial heterogeneity of the seismic response at Cusco and its potential relationship with the presence of a fault within the basin. Secondly, we focus on the influence of the urban environment on measurements and its implications for the assessment of local seismic response. Finally, we conclude with the perspectives opened up by this case study for reevaluating the seismic hazard of World Heritage sites in developing countries.

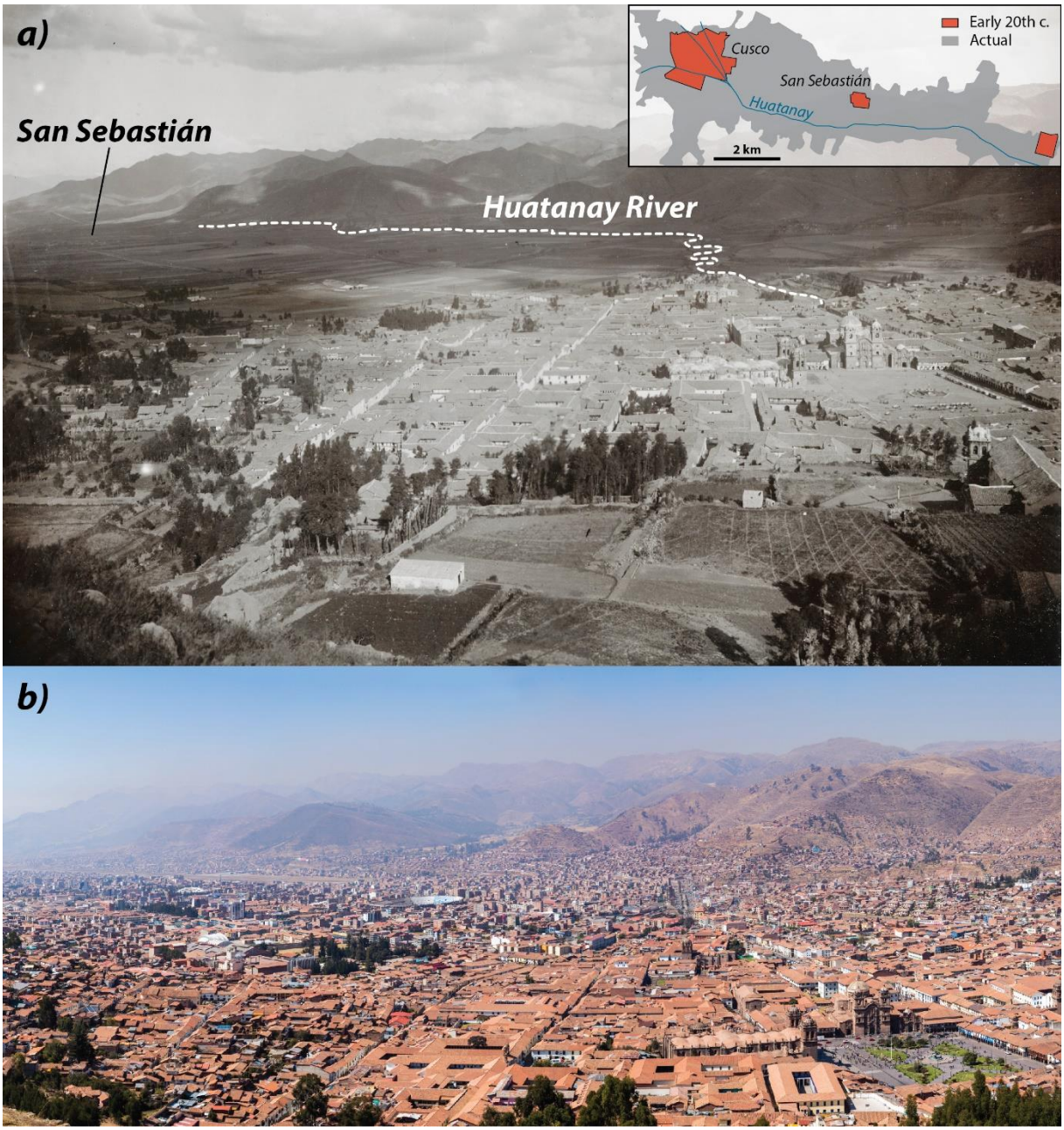

Fig.1 Cusco seen from Cruz Moqo a) at the end of the 19th century (picture of M. Uhle) and b) in 2015 (picture of D. Delso). You may note in a) the unchannelled course of the Huatanay River to the south of the city (white line). Credits: Ibero-Amerikanisches Institut & CC BY-SA 4.0. In inset, an overview of the urban sprawl from the beginning of the 20th century (modified from Alfaro et al. 2015)

2. The Cusco Valley, a rift basin prone to site effects

In the southern High Andes, most of the current deformation is accommodated at the interface between two lithospheric blocks (Carlier et al. 2005; Ma and Clayton 2014). These blocks are separated by a significant pre-existing structure, known as the Cusco Vilcanota Fault System (CVFS). Within the Cusco region, this system delineates the Eastern Cordillera from the Altiplano (Carlier et al. 2005) and manifests as a complex network of faults trending in a NW-SE direction (Fig.2a). Originally categorized as thrust faults, these structures have exhibited a transition to normal faulting since the Pliocene, approximately 5 Ma ago (Suárez et al. 1983; Sébrier et al. 1985; Cabrera 1988; Mercier et al. 1992). Abundant evidence now supports the Holocene activity of these faults, providing substantial insights into quantifying the present-day extensional regime.

Besides the existence of fresh scarps and offset moraines that constitute good geomorphological markers (Cabrera et al. 1991; Benavente et al. 2013; Rosell et al. 2023) and allow us to estimate a current rate of deformation of the order of 1 to 4 mm/year (Wimpenny et al. 2020), palaeoseismic trenches revealed events of moment magnitude (Mw) greater than 6 over the last 10,000 years (Cabrera and Sébrier 1998; Palomino et al. 2021; Rosell et al. 2023). Finally, the installation of a temporary seismological network to the north of Cusco recorded localized seismicity along the Qoricocha and Tambomachay fault planes (Fig.2; Guardia and Tavera 2015).

These tectonic structures and the current extensional phase led to the formation of intra-cordilleran basins. These semi-graben structures include the Cusco Valley, which was occupied by the vast Lake Morkill in the Pleistocene (Gregory 1916). The basin is now filled by a large quantity of fluvio-lacustrine and alluvial sediments that compose the San Sebastian Formation (SBF). The Cusco City Centre (CCC) is located at the north-western end of the sedimentary basin. It is located at the confluence of three seasonal rivers (Chunchullmayo, Huatanay-Saphy and Tullumayo; Fig.3), now channeled, which are responsible for a significant sediment input during the rainy season (Nuñez 2021) and a shallow piezometric level (Candia-Gallegos et al. 1993; INDECI-PNUD 2003). These Quaternary fillings are a major concern for assessing the seismic hazard. Depending on their nature, geometry and thickness, these formations will respond differently to earthquakes. Unfortunately, very little information is available on the exact nature, distribution, thickness and water saturation of the sediments of the SBF since no borehole has ever been drilled and, to our knowledge, only few geotechnical studies have been undertaken. These include a characterization of the soil types at the surface by Candia-Gallegos

et al. (1993) and Benavente Velásquez et al. (2004) who report the presence of sand and silts from alluvial and lacustrine origin in the city center. Non-invasive geophysical surveys involving seismic refraction, electrical techniques and MHVSR (INDECI-PNUD 2003; CISMID and UNI 2013; Barrientos 2021) were carried out, providing a rough image of the Cusco Basin only in its central part down to depths of ~150m. Finally, based on earthquake records from a temporarily installed accelerometer, Alcántara Torres et al. (2022) were able to estimate a natural frequency of 1.1 Hz in the CCC. For all these studies, only part of the data seems to have been published, making them difficult to review. As it stands, the heterogeneous San Sebastian Formation, composed of a succession of clay, gravel and unconsolidated sand horizons, is considered to be underlain by sandstones and conglomerates from the Paleogene (San Jerónimo group) as well as gypsum, limestone and shale formations from the Late Cretaceous (Yuncaypata group) outcropping to the north of the basin and dipping towards the southeast (Carlotto et al. 2011; Fig.2b). The thickness of the Quaternary formation is thus probably gradually increasing to the south-east, in the downstream direction.

This lack of information is a major shortcoming regarding the characterization of the soil dynamic response and the subsequent seismic microzonation of the site, particularly in the listed historical city center. The active faults that run through the region represent a significant hazard, and the potential amplification phenomena within the basin have yet to be addressed. Site effects were reported during the most violent historical earthquakes (1650: Mw>6; 1950: Mw~5.7; Fig.2a) and appear to be directly linked to the unconsolidated sediments of the basin. These include liquefaction phenomena in the form of mud volcanoes (Silgado et al. 1952; Villanueva 1970) and a significant rise in the water table (Ericksen et al. 1954; Ladrón de Guevara 1967). Interestingly, the highest seismic intensities in 1950 were mapped in the western part of the basin (Fig.2a).

In this rift basin, the sedimentary infill also appears to cover unmapped fault segments, which would represent an additional risk for the population. The Cusco fault (Fig.2), was first suspected by Carlotto et al. (2011). Since then, electrical tomography (Benavente et al. 2013) and magnetotelluric studies (Antayhua et al. 2021) have demonstrated its existence and its highly branched nature. Nevertheless, its Holocene activity has not been established and its exact trace remains to be defined.

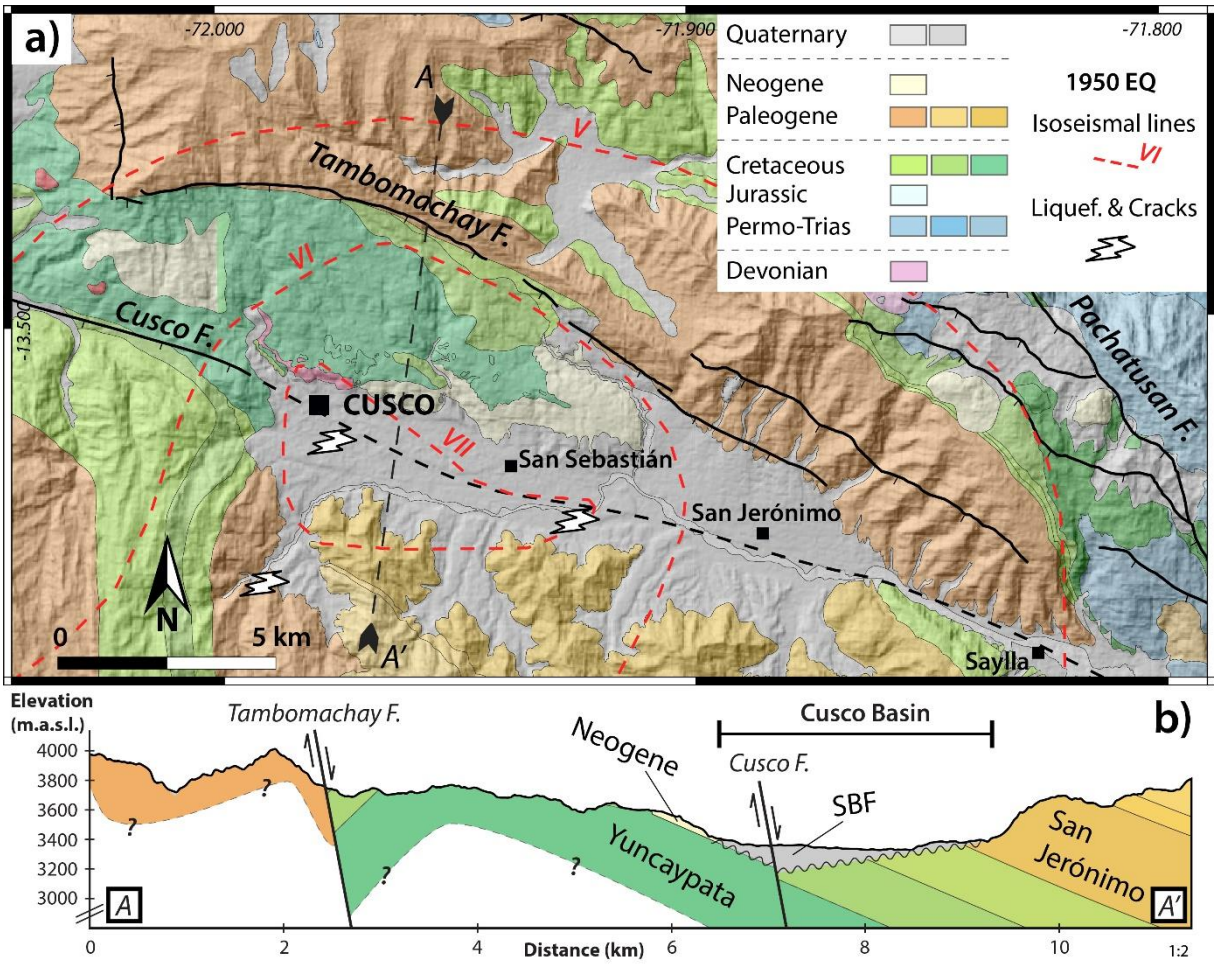

Fig.2 a) Geological map of the Cusco area (INGEMMET 1:100,000 Cusco sheets 27r, 27s, 28r and 28s). Active normal faults frame the Cusco Basin. After the 1950 earthquake, site effects (liquefaction and ground fissures) were reported in the west part of the basin. Isoseismal lines (in red) are based on Ericksen et al. (1954); b) Cross-section (AA') near the CCC. The subsurface geology is based on Carlotto et al. (2011).

3. Geophysical methods

In light of these concerns, two geophysical surveys were carried out in April and July 2023 as the joint initiative of French public research institutions (IRD, CEREMA) and the Geological, Mining and Metallurgical Institute of Peru (INGEMMET). The aim was to achieve complete coverage of the CCC using two distinct ambient vibration-based methods. These methods included single-station recordings using a short-band velocimeter to compute Microtremor Horizontal-to-Vertical Spectral Ratio (MHVSR), and a multichannel seismic survey to analyze the propagation of surface waves (Rayleigh) using the Microtremor Array Measurement

(MAM) technique. As the soil response depends mainly on the thickness of the layers, their geometry and their physical properties, it is directly linked to the propagation speed of shear waves (Vs). The passive seismic methods are cost-effective, non-invasive, and non-destructive, making them particularly well suited to the challenging urban context of Cusco (narrow streets, steep slopes, listed city). We first present the methodology of the single-station MHVSR survey, followed by a description of the multichannel array. Finally, we explain the joint inversion procedure for the results obtained from the two previous passive methods.

3.1. MHVSR survey

Ambient vibration (or microtremor) based methods consist of recording background seismic noise (natural and anthropic) to understand the properties and characteristics of the geological units (types of rock and sediment). Among these, the Microtremor Horizontal-to-Vertical Spectral Ratio (MHVSR) computes the ratio between the quadratic average of the horizontal and vertical Fourier spectra. This technique, popularized by Nakamura (1989), postulates that the frequency peak of the MHVSR corresponds to the fundamental frequency and the amplitude could serve as a "proxy" for the amplification factor of the site.

The MHVSR technique is considered a simple and effective method for characterizing the morphology and distribution of geological units. However, this method remains the subject of intense debate due to 1) its relevance only in perfectly horizontally stratified media (1D hypothesis; Mucciarelli and Gallipoli 2001) and 2) the insufficient knowledge regarding the exact contribution of different wave types to the generation of the H/V peak (Lunedei and Malischewsky 2015; Molnar et al. 2018). However, whether the peak is explained by the S-wave resonance frequency (e.g., Nakamura 1989), Rayleigh wave ellipticity (e.g., Lachet and Bard 1994), the Airy phase of Love waves (e.g., Konno and Ohmachi 1998) or a mix of all three (Bonnefoy-Claudet et al. 2008), the method has demonstrated its usefulness and accuracy (for a detailed discussion about the underlying hypothesis about the ambient wavefield characteristics, the reader is referred to Bonnefoy-Claudet et al. 2008). It has been particularly effective in investigating sedimentary basins and assessing the seismic site response, particularly in urban environments (e.g., Lebrun et al. 2001; SESAME 2004; Bonnefoy-Claudet et al. 2008; Pilz et al. 2009; Zavala et al. 2021; Pacheco et al. 2022). In practice, the MHVSR method is based on the assumption that there is a clear contrast of seismic impedance between the subsurface and the bedrock at depth. This difference in amplitude between the horizontal

and vertical signals in the upper layer is expressed as a peak at the soil fundamental frequency (f_0). The amplitude of the peak (A_0) depends on the impedance contrast between the underlying layer and the layer of interest. Besides the effect of the velocity/density contrast at depth, the MHVSR may also be affected by the Poisson ratio of superficial layers, the contact geometry and damping in the sediments (Lachet and Bard 1994; Lunedei and Malischewsky 2015).

We carried out 149 measurements throughout the CCC (Fig.3; Table S1) using portable three-component velocimeters Lennartz 3Dlite MkIII (short-band) and Guralp CMG40T (medium-band). These seismometers, with resonance frequencies close to 1Hz, have proven suitable for retrieving MHVSR peaks down to 0.2Hz (Strollo et al. 2008). All acquisitions were carried out using a MiniShark datalogger (Keas) configured with a sampling rate of 200 Hz and a minimum recording time of 20 minutes. The sensors were oriented to magnetic north and installed directly on the pavement (either concrete or asphalt). The signals were then processed with the Geopsy software (Wathelet et al. 2020). To generate the MHVSR curves, we used 40-second windows without overlap and tapered with a Tukey window. The spectral amplitudes were smoothed using the Konno and Ohmachi window with a relative width of 20% (b=40). According to Picozzi et al. (2005), processing data from recordings of at least 20 minutes in this manner ensures stable and representative results. Regarding sensor installation and signal analysis, we followed, as far as possible, the procedures and guidelines established by SESAME (2004) despite the inherent constraints of the urban context (e.g., inability to bury the sensor, proximity to buildings, vehicular traffic, etc.). In different parts of the city, we made sure to acquire data at different times of the day (4 am to 11 pm) and on different days in order to corroborate the stability of the results (Xu and Wang 2021; Molnar et al. 2022). No measurements were taken in strong winds. Before calculating the MHVSR curves, the quality of the measurement was checked using a preliminary analysis of the Fourier spectra. We checked that 1) the MHVSR peak resulted only from a decrease in spectral amplitude in the vertical component and 2) that no spurious peaks (due to coupling issues or anthropic sustained noise) were affecting the analysis. In addition, we checked that the three main criteria established by the SESAME (2004) protocol were satisfied (f_0 superior to at least 10 significant cycles in each window, a recording period covering at least 200 significant cycles and a standard deviation of the amplitude less than 2 close to the MHVSR peak). Points that do not meet these conditions (outliers) are not presented in this work.

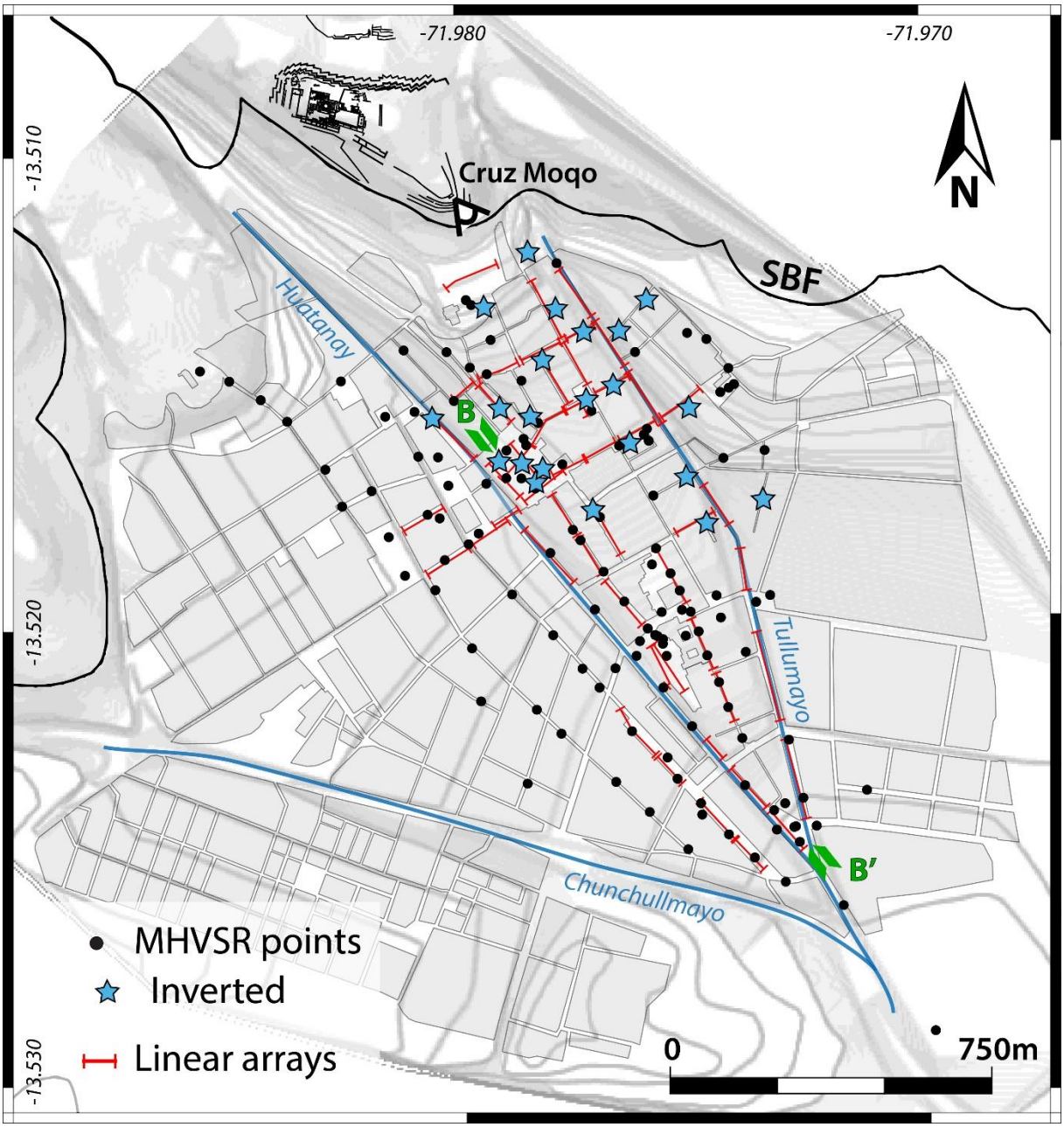

Fig.3 Map showing the location of the MHVSR measurements and linear arrays. Blue stars display the 22 MHVSR points that were considered for inversion. Green arrows indicate the BB' profile displayed in Fig.9. The dark line shows the upper limit of the San Sebastian Formation (SBF) provided by Carlotto et al. (2011). Credits DEM (Slope): Instit. Nacional de Cultura, Center for Advanced Spatial Technologies (Univ. Of Arkansas) & Cotsen Institute for Archaeology (UCLA).

3.2. Multichannel seismic recordings

Besides single-point recordings, we carried out multichannel acquisitions to estimate the propagation velocity of surface waves, and in particular to determine the shear wave velocity in the first 30 meters (Vs30). The propagation velocity characteristics of surface waves provide important information on the physical and elastic properties of the subsurface (Anderson et al. 1996). We designed linear arrays using a Geode (Geometrics) 24-channel seismograph and 24 Phasi 4.5 Hz geophones. The spacing between each geophone was 5 meters (total line length: 115 meters) but was reduced up to 3 meters (69-metres line) for the needs of some acquisitions. We used the equipment following the Microtremor Array Measurement (MAM) technique based on the Spatial Autocorrelation (SPAC) method. The minimum recording time was 20 minutes and the sampling frequency of the geophones was set at 50 Hz. In order to avoid heavy vehicular traffic (particularly buses), measurements were preferably conducted during the quietest hours, at sunrise and late in the evening. In total, 50 seismic lines were recorded (Fig.3; Table S2). The S-wave dispersion curves of the fundamental mode (Rayleigh wave phase velocity) derived from the recordings were plotted using the proprietary software SeisImager (Geometrics). Vs30 values for each linear array were then computed using the software Geopsy. In addition to the linear arrays, we designed a 100-m diameter circular array in the main square of Cusco (*Plaza de Armas*) using 6 Lennartz 3Dlite MkIII velocimeters and a Cityshark datalogger (Fig.4a-b). Two 40-minute recordings were made at a sampling frequency of 200 Hz. The dispersion curve was extracted using the frequency wavenumber analysis (F-K tool) in Geopsy.

3.3. Calibrated joint inversions

Once the MHVSR and Rayleigh waves dispersion curves have been computed, the aim is to estimate the subsurface S-wave velocity structures and the sediment thickness beneath the CCC. To do so, we carried out joint inversions of the two datasets using the freely available software HV-inv (García-Jerez et al. 2016). By reducing the model search space, joint inversions allow for better fitting the observed data and retrieving a more reliable model of the local velocity structure (e.g., Parolai et al. 2005; Picozzi et al. 2005b). We estimated the best-fitting model following 3,000 iterations and we allowed the model parameters to vary within ± 5% search space of the initial model (guided Monte Carlo method). Based on the available geological data

(INDECI-PNUD 2003; Carlotto et al. 2011), we considered 4-layer models with the following parameters:

- 1st layer: upper part of the soft Quaternary sediments from the SBF. Vs between 150 and 500 m/s, depth constrained to 100m and density between 1500 and 2000 kg/m^3;
- 2nd layer: lower part of the soft Quaternary sediments from the SBF. Vs between 200 and 600 m/s, depth constrained to 100m and density between 1500 and 2000 kg/m^3;
- 3rd layer: considered as a theoretical "engineering bedrock" with a Vs of 700 to 1200 m/s (Gupta et al. 2021), a maximum depth of 300m and a density of 2000 to 2500 kg/m^3;
- 4th layer: Vs greater than 1000 m/s, infinite depth and a density of between 2200 and 2500 kg/m^3.

We first inverted the passive seismic array data recorded on the *Plaza de Armas* using two independent measurement techniques (at different times and days). On one hand, we used the dispersion curve computed from the circular array and the MHVSR curve obtained from the station at the center (R1). On the other hand, we considered the data from a linear array cutting across the main square (L54) and the MHVSR point P36 located near the center of the circular array (Fig.4b). Given the stability and consistency of the results (Fig.4c-d), we inverted the subsurface velocity model for 22 separate measurement points in the northern part of the CCC (Fig.3, Table S3), where we identified a strong MHVSR peak. For 17 of these points, we performed the joint inversion of MHVSR and MAM data recorded at the same location. For the remaining 5 points where no multichannel measurements were available, we used only the MHVSR curve.

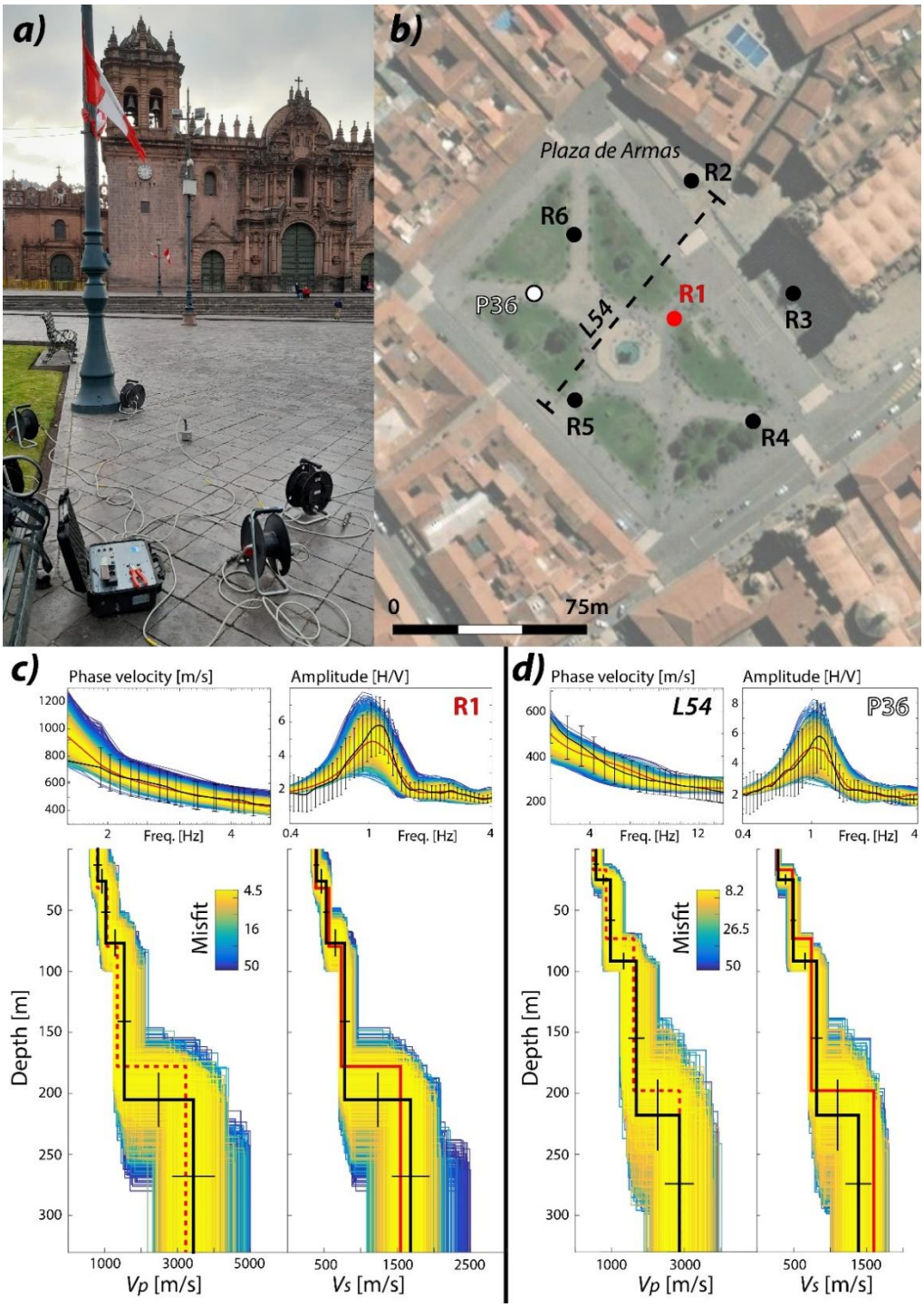

Fig.4 a) Equipment used for the 100m diameter array; b) Circular setup of the array as well as the MHVSR point (P36) and linear array (dotted line L54) considered in d); c) Velocity models resulting from the combined inversion of the S-waves dispersion curve and MHVSR curve (R1) of the circular array (top left and top right respectively); d) Velocity models resulting from the combined inversion of the S-waves dispersion curve of L54 and the MHVSR curve of P36 (top left and top right respectively). Black curves represent the experimental data and its standard deviation. Red lines indicate the best fitting models.

4. Results

4.1. Experimental data

For single-point measurements, we picked the frequency (f_0) and amplitude (A_0) of the MHVSR peak. In 119 out of 149 cases, we identified a peak (Table S1), while in 7 cases, the MHVSR curve showed a ratio close to 1 over the frequency range 0.4-10 Hz. These points were interpreted as outcropping bedrock. Finally, for 22 measurement points, not randomly distributed, it was not possible to pick out a precise peak. This was due to either 1) a sharp increase in the MHVSR at low frequencies (<1 Hz) and/or 2) a "plateau" present at low frequencies ending more or less abruptly around 1 Hz (Fig.5a-b). The curves of these points differ markedly from the 7 recordings interpreted as outcropping bedrock in their low-frequency content and are generally located in the middle of the Cusco Basin, making the hypothesis of an outcrop very unlikely.

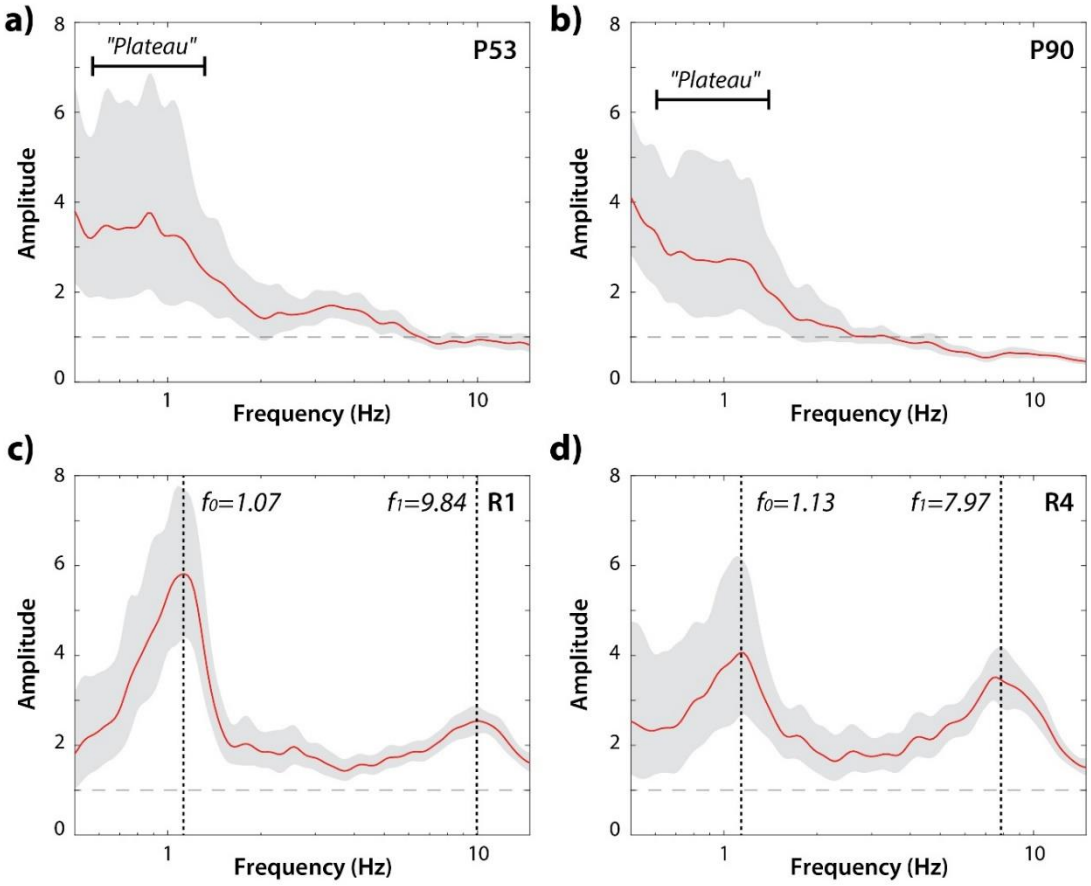

Fig.5 MHVSR curves (red lines) and their respective standard deviations (grey area) of four measurement points. In a) and b), the strong increase of the amplitude values and the “plateau” below 1 Hz makes it impossible to determine a f_0. c) and d) Two examples of MHVSR curves recorded in the *Plaza de Armas* and showing a secondary peak with distinct f_1 and A_1.

Figure 6 shows the distribution of the fundamental frequency (f_0) interpolated using the Triangular Irregular Network (TIN) method from the QGIS package. Despite the usually large standard deviation of MHVSR ratio for frequencies below 1Hz – likely due to the challenging context of the urban environment (ground coupling, diversity of noise sources) and the use of short/medium-period sensors (1s) – the results of the f_0 picking show a very good spatial coherency. The f_0 value is generally associated with the depth at which a strong impedance contrast exists (Molnar et al. 2018), such as the interface between unconsolidated Quaternary sediments and a more competent basement. In the case of the CCC, the results of the MHVSR survey support this hypothesis. The rapid decrease of the f_0 value (from 4 Hz to 0.6 Hz) from the edge of the basin in the north towards the middle of the valley in the south corresponds most probably to a deepening of this interface under the soft Quaternary sedimentary cover. Likewise, the outcropping bedrock is identified to the north-east of the CCC at the top of the steepest part of the study area, near the limit of the San Sebastian Formation as displayed in Figure 3 (Carlotto et al. 2011). In the *Santo Domingo* sector, however, f_0 values appear to decrease more rapidly (Fig.6), in accordance with a sudden deepening of the interface. In this respect, the 22 MHVSR measurements showing no peaks (red crosses in Fig.6) and distributed along a line oriented more or less NW-SE, seem to delimit this area to the north. At first sight, these measurements suggest the disappearance of the impedance contrast at depth.

While f_0 is mainly related to the depth of the impedance contrast, the amplitude A_0 of the peak depends on the impedance contrast between the upper and underlying layers (Albarello and Lunedei 2011). The higher the amplitude, the greater the impedance contrast. Unlike f_0, A_0 appears to have a much more heterogeneous and complex distribution (Fig.7). The north-western part of the CCC has low amplitudes ($A_0 \leq 3$), while sectors of the *Plaza de Armas* and *Santo Domingo* have higher amplitudes ($A_0 > 5$).

Finally, it should be noted that for 54 measurements, it was possible to identify a clear secondary peak (*f1*) corresponding to either a harmonic of the natural frequency of the site or a shallower impedance contrast (Fig.5c-d). The frequency exhibits very high variability, ranging from 1.5 to 19 Hz (Table S1). The amplitude of this second peak (A_1) remains low, usually less than 3.

Meanwhile, the Vs30 calculated from the 50 linear arrays range from 250 to 480 m/s (Table S2) suggesting the presence at the subsurface of significant "deposits of dense or medium dense

sand, gravel, or stiff clay" (soil type C, Eurocode 8, 2005), consistent with the geological description of the SBF. Once again, there is a north-south trend, with a significant drop in velocity between the *Plaza de Armas* and the *Santo Domingo* sector (Fig.6-inset).

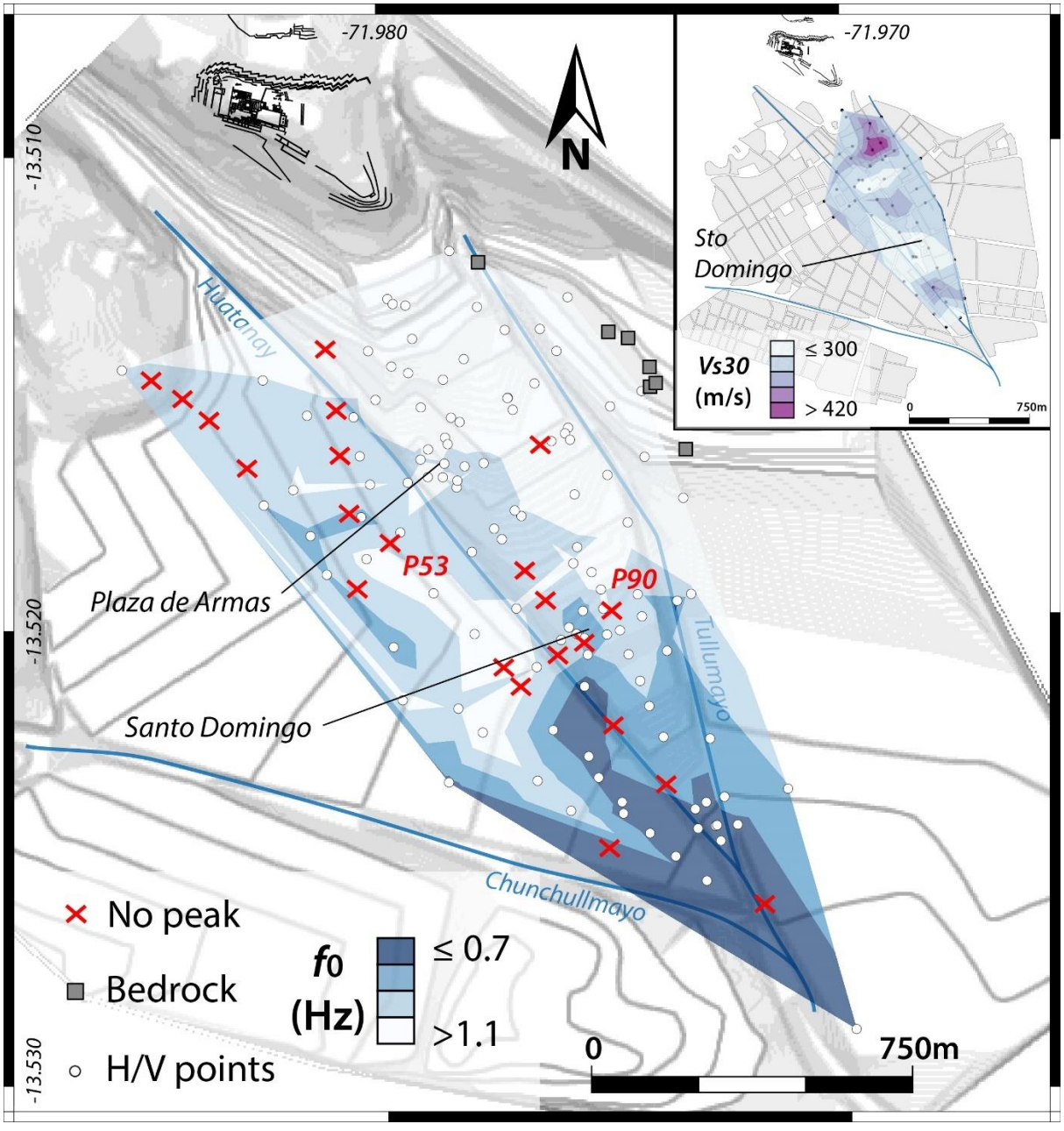

Fig.6 Distribution of the MHVSR fundamental frequency (f_0). Red crosses indicate measurements where we were unable to identify a peak. In inset, the Vs30 distribution in the CCC. Credits DEM (Slope): Instit. Nacional de Cultura, Center for Advanced Spatial Technologies (Univ. Of Arkansas) & Cotsen Institute for Archaeology (UCLA).

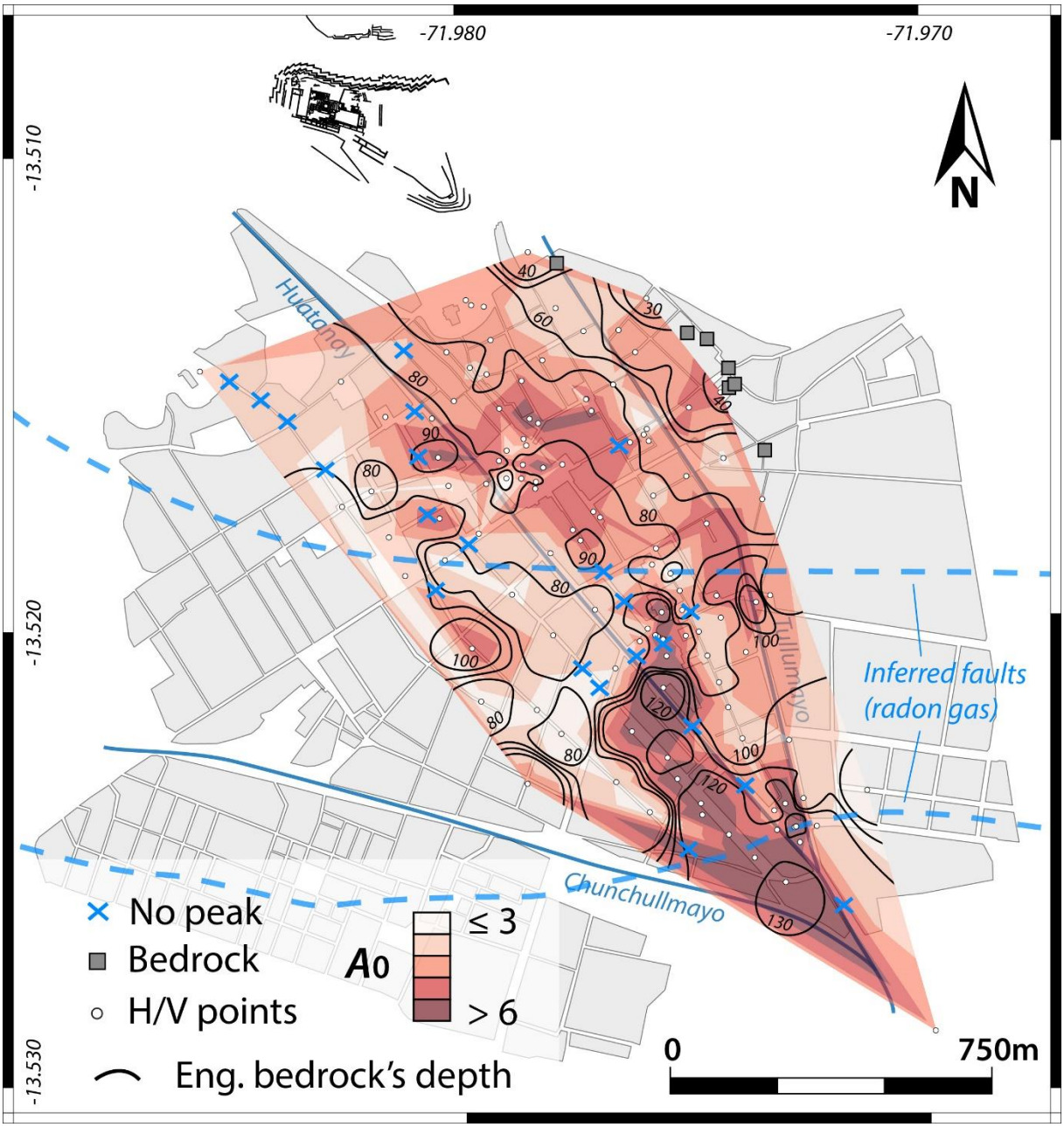

Fig.7 Engineering bedrock depth's contour map of the CCC compared to the distribution of the amplitude of the first peak (A_0). High amplitudes are preferentially associated with the deepest part of the basin. The blue dotted lines indicate the fault traces inferred from anomalous radon concentrations (courtesy B. García).

4.2. Subsurface velocity model

Could the site response provide information about the structure and physical properties of the subsurface? We combined the results of the multichannel recordings with those of the MHVSR points to derive velocity models at several locations in the CCC. Firstly, we wanted to assess the consistency of the results by comparing the velocity models of the main square of Cusco using two different techniques. A first velocity model was obtained by the joint inversion of the S-wave dispersion curve resulting from the circular array and the MHVSR curve coming from the station at the center of this network (R1). A second model was based on the inversion of the dispersion curve of a linear array crossing the square (L54) from west to east and a nearby MHVSR point (P36). It must be noted that both data acquisitions were not done simultaneously. Figure 4 shows the design of the different geophysical surveys (Fig.4b) as well as the outputs of the two inversions (Fig.4c and 4d). Both inversions exhibit low and similar misfit values, indicating the same subsurface structure: two first layers with low Vs (< 500 m/s) followed by a more competent layer (Vs > 700 m/s) at a depth of around 70 m and with a significant thickness of 100 to 150 m (Fig.4 c-d). We then observe another significant velocity rise (Vs > 1500 m/s) at greater depths (> 150 m). With Vs greater than 700 m/s, the third layer will hereafter be referred to as the 'engineering bedrock' (Gupta et al. 2021).

Given the consistency of the results at the *Plaza de Armas*, the same procedure was applied to 21 other points in the CCC, including 17 where both an MHVSR curve and a dispersion curve derived from a linear array were available. All the points were selected in the northern part of the city (Fig.3). As the frequency of the MHVSR peak is relatively high there, the dispersion curves derived from the MAM were all the more relevant for constraining the inversion down to the first impedance contrast. By averaging the shear wave velocities and depths of each of the four layers from the best-fitting models, it is possible to generate a unidimensional CCC velocity model (Fig.8a). The model thus obtained supports the existence of the first two layers with similar thicknesses (~ 30m) and relatively low shear wave velocities (Vs ~ 300 and 500 m/s respectively). Underneath, there is an initial rise in Vs corresponding to the engineering bedrock (~ 800 m/s). This third layer, approximately 150 m thick, overlays a much more competent fourth layer, highlighted by a new rise in shear velocity (Vs > 1400 m/s). The results of the 22 inversions are therefore entirely consistent with the two models obtained at the Main square. Note the limited dispersion of the velocity values compared with the degree of freedom left to the models (Fig.8a). As an illustration, the mean and standard deviation of the Vs of the engineering bedrock is 823 ± 94 m/s. Only the parameters of the fourth layer appear to be less

well constrained. The explanation lies in the uncertainty and low resolution of the methods used at low frequencies (f ≤ 0.6 Hz). Depths of the engineering bedrock obtained from the best-fitting models were then compared with the f_0 of the inverted MHVSR curves (Fig.8b). The fitting of a power law function gives: $Z= 86.34 f_0^{-0.777}$ (R^2=0.79), where Z refers to the depth of the engineering bedrock, and f_0 to the fundamental frequency of the site. Although the power law relationship indicates some variability in the physical properties of the overlying layers (OL), the relationship proves to be close to the theoretical relationship f_0 = Vs/4H (Nakamura 2000) or $H_{OL}=(Vs/4)*f_0^{-1}$, where H_{OL} and Vs correspond to the thickness and S-wave velocity of the overlying layers. This demonstrates that the shape and frequency of the MHVSR peak is mainly driven by the first impedance contrast between the second (Quaternary sediments) and third layers (engineering bedrock: Late Cretaceous and Paleogene formations). Despite the contrasts in terms of A_0 and Vs30 highlighted between the northern and southern parts of the CCC, we decided to assume a relative geological homogeneity (horizontal continuity) throughout the Cusco city center. As a result, we computed the depth of the engineering bedrock based on the above power law function, wherever a value of f_0 was available. In other words, it enables to assess the variation in thickness of the unconsolidated sediments beneath Cusco, which is a key concern in many geo-engineering studies (e.g., Lebrun et al. 2001; Abbaszadeh Shahri et al. 2021; Pacheco et al. 2022). Figure 7 shows the engineering bedrock isodepth contour lines based on the interpolation of the computed depth values using the Inverse Distance weighting (IDW) method (QGIS package). Mirroring the f_0 distribution, the engineering bedrock depth increases towards the south. From 40 meters in the north, the engineering bedrock is estimated to be more than 120 meters deep in the southern part of the CCC. In the sector of *Santo Domingo*, the engineering bedrock seems to sink severely by almost 30 meters in less than 50m of horizontal distance.

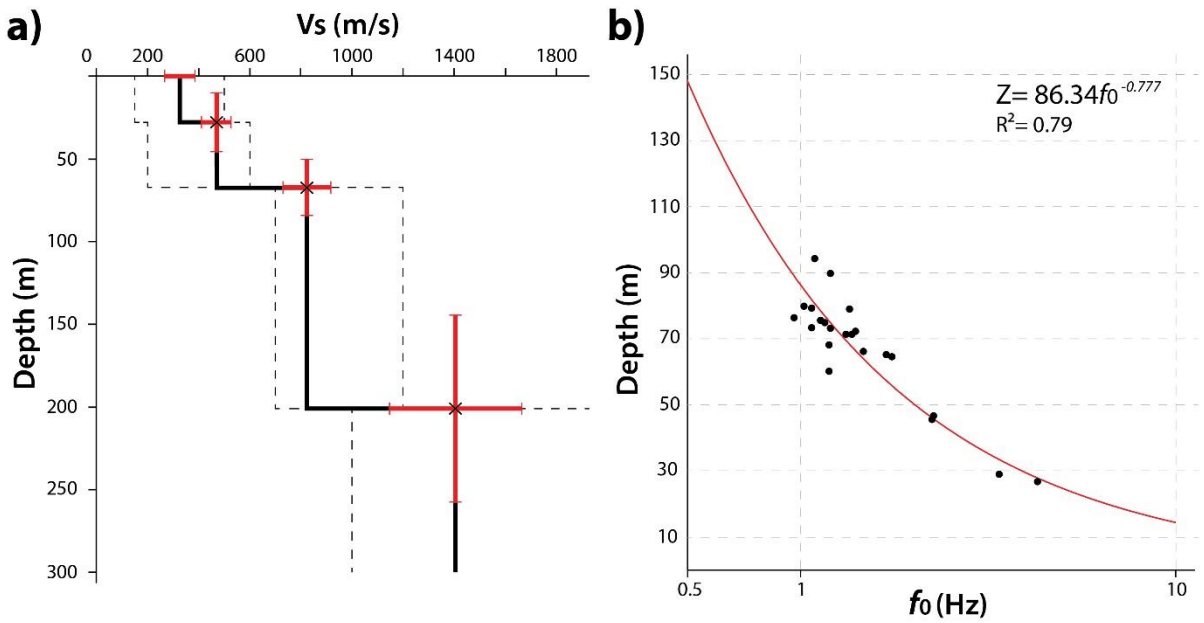

Fig.8 a) Theoretical shear wave velocity model inferred from the mean depth and Vs of each layer of the 22 inverted points. The dotted lines indicate the model search space; b) Relationship between the fundamental frequency and the inverted depth of the engineering bedrock for 22 MHVSR points in the northern part of the CCC.

5. Discussion

5.1. Tracking the Cusco fault below the CCC

The velocity model (Fig.8a) is in good agreement with the results of the electrical resistivity survey carried out previously to the south of the CCC (INDECI-PNUD 2003). Their authors estimated the contact between soft sediments and more compact rocks belonging to the San Jeronimo Group (Eocene) at a depth of around 50-60m. Our results for the CCC indicate a similar structure: several horizons of the San Sebastian Formation, at least 40m thick and constituting the basin infill, overlie Eocene formations visible to the south of the basin and/or Cretaceous formations outcropping to the north of the basin (Yuncaypata Group; Carlotto et al. 2011). In any case, based on Vs values, the engineering bedrock would consist of significantly altered sandstone or limestone formations. Aside from this simplified geological model, the data from this geophysical survey highlights some particular features.

As pointed out in the previous section, the variations of natural frequencies seem to be strongly correlated with the geometry and depth of the first impedance contrast (Fig.8b), referred to as the engineering bedrock. In other terms, the quick and strong decrease of the f_0 that we observe

in the southern part of the CCC suggests a sudden steepening of the engineering bedrock close to the *Santo Domingo* sector (Fig.7). The sudden thickening of the sediment cover in that area is hard to explain without the existence of geological structures or discontinuities. Several studies have provided evidence of the existence of a fault, named hereafter the Cusco fault, running parallel to the basin (Carlotto et al. 2011; Benavente et al. 2013; Wimpenny et al. 2020). While field observations report the presence of deformed Quaternary sediments within the basin (Benavente et al. 2013), electrical resistivity profiles reveal colluvial wedges (Benavente et al. 2013). Since then, magnetotelluric profiles carried out by Antayhua et al. (2021) have confirmed the tectonic origin of the Cusco Basin and suggested a branched structure with several fault segments connected at depth.

Our findings seem to attest to the presence of at least one fault segment beneath the CCC and thus offer interesting avenues for research into the influence of tectonic structures in modifying the local ambient noise wavefield. We base our analysis on the recent work of García et al. (in prep.), who mapped radon gas anomalies in the Cusco area and matched them to the active faults in the area. The authors found several well localized anomalies distributed linearly and parallel throughout the Cusco Basin (García et al. pers. comm.). The authors therefore support the existence of several parallel fault segments, oriented NW-SE across the basin. It turns out that among the areas showing anomalous radon concentrations, several are located in the *Santo Domingo* sector and at the confluence of the Huatanay and Chunchullmayo rivers (*Pumacchupan*). The presence of a normal fault in the *Santo Domingo* sector is perfectly consistent with the results of this work. As shown in Figure 7, the area of sudden deepening of the engineering bedrock to the south of *Santo Domingo* agrees very well with the fault line proposed by García et al. (pers.comm.). The map also highlights the strong spatial agreement between the variations in amplitude of the MHVSR peak (A_0) and the breaks in slope of the engineering bedrock. Given the influence of the impedance contrast's geometry on the amplitude of microtremor measurements (reflection, refraction, complex surface wavefield; Irikura and Kawanaka 1980), it is likely that a geological discontinuity, i.e. a fault zone, could affect the MHVSR peak locally (Mucciarelli et al. 1999; D'Amico et al. 2008; Tarabusi and Caputo 2017; Tibaldi et al. 2024). Indeed, it is in this zone of lower amplitude that most of the MHVSR curves, for which no f_0 value could be picked, are located. Regarding the higher uncertainty of the MHVSR measurements at these points, we should point out that the large standard deviation cannot be solely explained by the relatively short recording period (~20 min)

and the non-stationary nature of the ambient vibrations. At various measurement points, a longer recording duration (40 min) gave similar results.

Looking at a N-S profile (Fig.3 and 9), some of the MHVSR curves (2 and 4) show very local shrinkage (reduction of A_0) and/or broadening (plateau) of the peak, which makes more difficult to estimate the f_0. Strikingly, the areas in which these two points are located correspond to the assumed traces of two fault segments based on radon gas measurements (Fig.7 and 9). The sectors between points 1 and 3 and between 3 and 5 also show a more or less sudden drop of f_0. The MHVSR method is not meant to identify faults. Although MHVSR surveys have already been used to identify and locate tectonic structures, the discussion was limited to sudden variations in f_0 (D'Amico et al. 2008; Stanko et al. 2017; Tarabusi and Caputo 2017; Khalili and Mirzakurdeh 2019) and wave polarization in the horizontal components (Lombardo and Rigano 2006; Pischiutta et al. 2013). To our knowledge, no work has ever addressed a potential disturbance of the wave field in the vicinity of an active fault that would significantly affect the MHVSR curves, excluding the preliminary observation made by Mucciarelli et al. (1999) in Italy. In short, the microtremor measurements, combined with the inverted velocity model, reveal a geological discontinuity, consistent with the trace of one segment of the Cusco fault. The concordance of areas without a clear MHVSR peak with the sudden deepening of the bedrock argues for an effect of this structure on the physical properties of the sediments in these areas, potentially generating disturbances in the wavefield. This fault with a normal component and dipping towards the south would displace the compact Eocene or Cretaceous formations but could also affect the overlying sediments, as evidenced by the disturbances in the MHVSR curves close to the discontinuity (e.g., colluvial wedge, fault gouge). Of course, these conclusions are still preliminary, as there is still a serious lack of other types of geotechnical and geophysical studies in the Cusco Basin. It is only through the combined use of complementary techniques such as radon gas measurements (García et al. in prep.), magnetotellurics (García et al. in prep.), ground-penetrating radar and InSAR that it will be possible to validate these results with any degree of certainty.

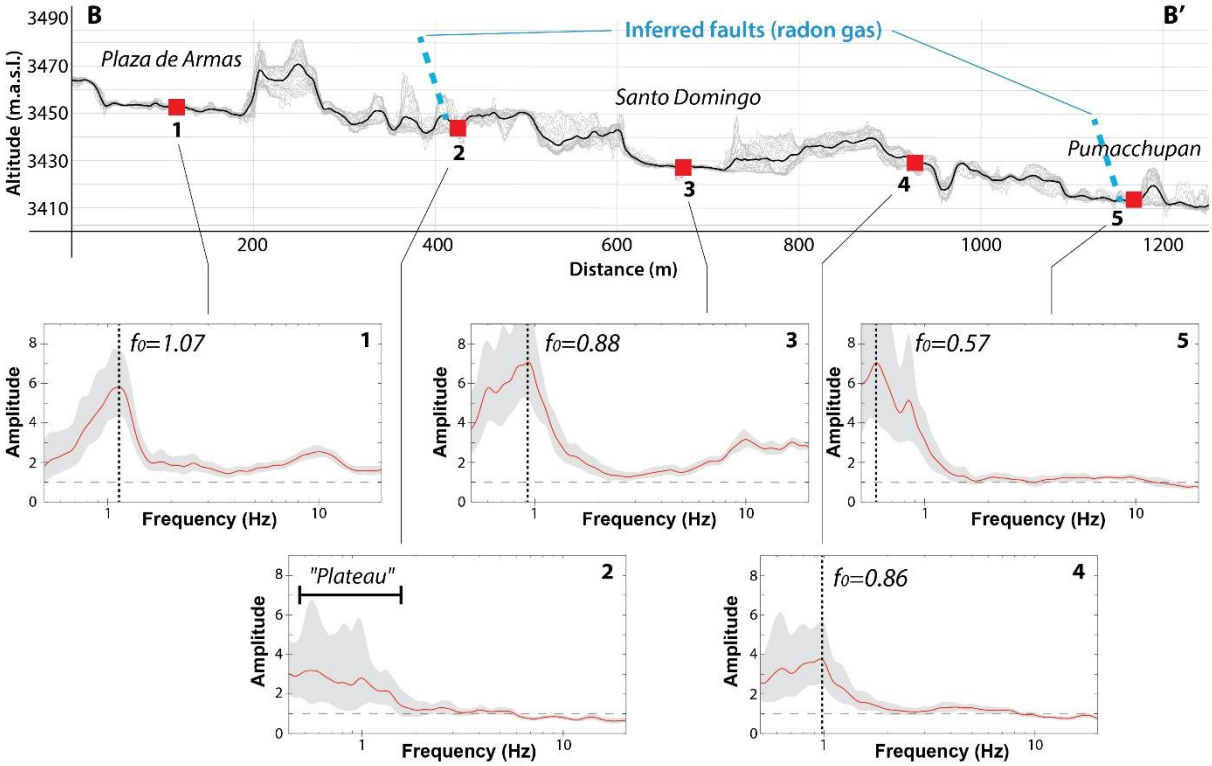

Fig.9 Swath profiles (40m width) between B and B' (Fig.3) derived from a high-resolution DEM (1.5 m) based on Pleiades images. The black curve displays the mean values. In the bottom part, the diagrams show the MHVSR curves (red lines) and their respective standard deviation (grey area) for five points located along the profile line. Note the sharp drop of the fundamental frequency of the peak between points 4 and 5. In blue, the proposed fault traces shown in Fig.7.

5.2.Urban environment: a masking effect for soil response evaluation?

Several studies have demonstrated that the MHVSR technique tends to underestimate the seismic amplification of a site, particularly in terms of the amplitude of the frequency peak (Lebrun et al. 2001; Pilz et al. 2009; Rong et al. 2017) and might only be regarded as a lower bound of the actual site amplification (Bard 1999; Bonnefoy-Claudet et al. 2006, 2008). Furthermore, the challenging nature of ambient vibration-based surveys in urban environments (Pacheco et al. 2022) and the non-linear response of the ground during strong transient shaking should not be overlooked. Nevertheless, as the frequency of the MHVSR secondary peaks falls within the frequency range of engineering interest (~3-10 Hz), it is necessary to examine the distribution and amplitude of these peaks in order to identify potential soil-structure interaction phenomena. Because of the wide variability of the f_1 frequencies identified during the MHVSR

survey, it is difficult to establish the origin of these peaks. They might be harmonics of the fundamental frequency f_0 or the expression of a shallow seismic interface within the Quaternary sediments of the San Sebastian Formation. Nevertheless, it is worth noting that the results of the joint inversion support the existence of a first moderate velocity contrast at a depth of around 30m, which is compatible with the lowest f_1 values (~5 Hz).

Given the densely urbanized environment in which the MHVSR measurements were carried out and the relatively small number of recordings showing an identifiable secondary peak (54, i.e., 1/3 of the total; Table S1), we are inclined to consider the role of shallow velocity inversions detailed by Castellaro and Mulargia (2009). The authors highlight the dramatic effect that very thin and stiff artificial layers (concrete/pavements) can have on the MHVSR curves, lowering the peaks down to relative low frequencies (~2Hz). These shallow velocity inversions are frequently accompanied by MHVSR curves with an amplitude below 1 over a wide range of frequencies. We observe this phenomenon on some curves, such as P90 (Fig.5b) and curve 2 in Figure 9. However, as the measurements were all carried out on paved areas, we should expect a generalized alteration in the MHVSR curves throughout the entire CCC. Actually, the f_1 distribution does not seem to be random and the amplitudes (A_1) do not seem to be damped out homogeneously. There is a clustering of the lowest values of f_1 ($\leq$ 5 Hz) on the margins of the city center, while most of the frequencies between 5 and 15 Hz are located in the core of the city (between the Tullumayo and Huatanay rivers). It should also be noted that the f_1 > 5 Hz generally has higher amplitudes than the $f_1 \leq 5$ Hz, which are characterized by very low amplitudes (< 2). In addition, the highest amplitudes (> 3) are confined to two sectors of the CCC: *Plaza de Armas* (Fig.5c-d) and *Santo Domingo*. These two areas exhibit two of the largest open spaces in the CCC. With regard to this singular f_1 distribution, we formulate two hypotheses, not mutually exclusive:

- A contribution of the Inca urban pattern in the differential response of the CCC;
- A masking effect of the city building network on the local site response.

The CCC is located on the exact place where the capital of the Inca Empire was settled in the 15th and 16th centuries, of which many remains can still be admired. At that time, the city's residential sectors were mainly confined between the Tullumayo and Huatanay rivers (Beltrán-Caballero 2013; Vranich et al. 2014; Bauer 2018), while an extensive network of agricultural terraces and canals structured the surrounding area (Fig.10). The *plaza de Armas* then represented half of a large open space known as *Hawcaypata*, while the sector of *Santo Domingo* consisted of a plaza to the north (*Intipampa*) and a terraced garden to the west,

bordering the Huatanay River. Given the long period of occupation of the city of Cusco (at least since the 11th century; Bauer 2018) and the great capacity of the Incas to transform their landscape (e.g., Wright 2006), it seems very likely that the Inca city of Cusco was made up of a large number of man-made earthworks. These embankments and terracing projects, which were potentially more extensive and thicker in the residential area, are also documented by Spanish sources describing the large quantities of sand brought in from other regions of the Empire to prepare the *Hawcaypata* square (Polo de Ondegardo 1916). The higher frequencies observed in the city core would therefore indicate the persistence of significant anthropogenic backfills, while on the periphery the absence of such deposits sometimes highlights a deeper impedance contrast (f_1 < 5Hz) between natural Quaternary horizons (Fig.10). The pre-Columbian urban planning and the past cultural practices could therefore be related, at least partially, with the f_1 distribution pattern. This hypothesis will have to be confirmed by further analysis of the archaeological data and stratigraphy.

A second hypothesis concerns the influence of the current urban layout on the site response. It has been established that buildings and their interaction with the ground can have a significant impact on nearby free-field measurements (Gallipoli et al. 2004). At the scale of an urban context, this "site-city seismic interaction" might significantly affect the site response in case of an earthquake. For Gueguen et al. (2002), the urban environment should not only be considered as a vulnerable entity but also as an active component of the seismic hazard. During an earthquake, building vibrations can be transferred back to the ground through the foundations (inertial soil-structure interactions), amplifying and prolonging the ground motion. In the case of the Mw 7.3 earthquake in Mexico (1995), the authors demonstrated that a high building-to-soil kinematic energy ratio usually implies high buildings, a high urban density and a correspondence between the site response and the building resonance frequencies. Although the previous work focuses on the “site-city interaction” during earthquakes, we can question the role of the urban layout of Cusco in contaminating the response of the site during a passive survey using MHVSR measurements. As proposed by Brûlé et al. (2017), cities can be regarded as metamaterials. In geophysics, such a concept implies that the urban fabric might behave like a group of “Above-Surface resonators” (Brûlé et al. 2020), modifying thus the response of individual structures and acting as surface wave filters (Colombi et al. 2016; Gueguen and Colombi 2016). It is striking that, despite the relative coherence of the frequencies of the secondary peak within the core of the city, the strongest amplitudes are restricted to the largest open spaces and therefore to the areas furthest away from buildings (Fig.10). In Cusco, most of

the buildings that make up the historical center are large colonial complexes with patios, connected to each other and subdivided over time into multiple flats and lots. Clustering effects and interactions between the structures are therefore likely to be high, and the data collected so far as part of our research suggests that modes specific to an entire residential block could be identified. The long-period vibrations of these ‘meta-structures' could thus alter the apparent response of the ground (Fig.S1).

In short, the clustered distributions of f_1 and A_1 do not seem to be explained solely by a velocity inversion at very shallow depths. They also point to a decisive role of the urban layout (past and present) in the response of the site. Although these hypotheses remain to be ascertained, the strong contrast in frequency between the core and the periphery could be due to differences in the nature and thickness of the surface sediments. The higher frequencies in the urban core could be associated with anthropogenic backfills dating from the pre-Columbian period, which are absent from the outskirts. In parallel, the strong contrast in A_1 between the open spaces and the rest of the city suggests a significant influence of the city's buildings on MHVSR measurements at medium and high frequencies (>3 Hz). If confirmed, the influence of these two parameters should be taken into account in a future microzonation of the city of Cusco.

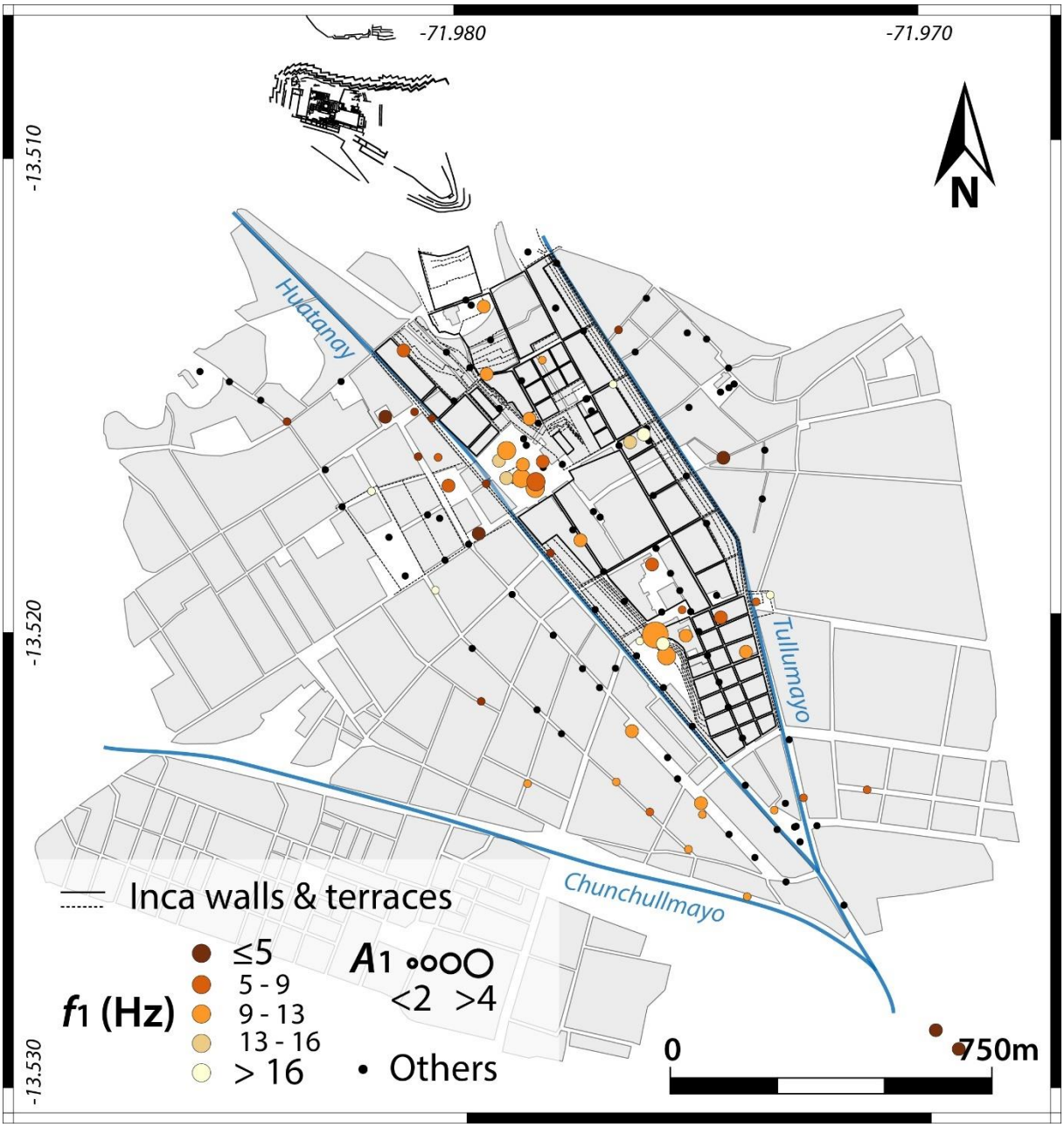

Fig.10 Value and amplitude of the MHVSR second frequency peak (f_1). The peak is present mainly in open spaces of Cusco.

6. Conclusions

As the impact of earthquakes on World Heritage sites "is well beyond the direct economic losses" (Despotaki et al. 2018), a better assessment of the seismic hazard and risk are crucial concerns for a developing country like Peru. Established in a tectonic basin prone to site effects, the “archaeological capital of the Americas”, Cusco, represents an emblematic case of vulnerable World Heritage city as well as of the many aggravating factors specific to Southern

countries (fast-paced urbanization, few geotechnical studies, heterogeneity of building conditions). The aim of this work was therefore to characterize the dynamic properties of the subsoil in the historical center of Cusco for the first time, and to pave the way for a seismic microzonation of the city. To tackle the inherent challenges of the urban environment, we relied on passive seismic methods, which offer rapid, cost-effective and non-invasive solutions.

Joint analysis and inversion of data acquired by single-station and array measurements using the MHVSR and MAM techniques enabled us to characterize the geometry and physical properties of the subsurface. The results therefore provide a good assessment of the fundamental frequency of the site and the variation of the sediment thickness at the scale of the urban center. The results indicate a rapid thickening from north to south of the unconsolidated Quaternary sedimentary cover (Vs < 400 m/s), from around 30 to almost 120 meters. All of the geophysical data, from the frequency and amplitude of the MHVSR peak to the Vs30 values, highlights a strong contrast between the northern and southern parts of the city center, supporting the existence of a geological discontinuity between the main square and the *Santo Domingo* sector. This discontinuity echoes the already documented presence of a normal fault running through the Cusco Basin. Moreover, there is a very good correspondence between the discontinuity identified in this work and the fault traces inferred from recent radon gas measurements (García et al. in prep.).

In addition, although the response of the Cusco subsoil seems to be mainly influenced by the interface between the bottom of the basin (engineering bedrock) and the sedimentary infill composed of fluvio-lacustrine sediments, the MHVSR survey suggests the existence of a second impedance contrast at a shallower depth (< 30m) in the core of the historical city of Cusco. Given the peculiar distribution of f_1, we assume that this secondary peak may be of human origin, corresponding to the earthworks carried out by pre-Columbian populations. The significantly higher amplitude of this frequency in the only two large open spaces also argues for a significant influence of buildings and the current urban layout on the elastic response of the subsoil.

These findings, though still hypothetical, could have a major impact on the assessment of the seismic vulnerability of the built heritage of the CCC. As the MHVSR method does not provide a reliable assessment of site amplification, this work was not intended to provide a quantification of site-effects amplifications. Nevertheless, the data acquired concerning the structure of the basin and the distribution of frequencies demonstrates the relevance of this approach for the necessary characterization of the subsurface of a UNESCO-listed city. Future

monitoring initiatives are promising. In a city like Cusco, where the water table seems to be shallow and subject to significant variations due to seasonal rainfalls, it would be particularly interesting to track natural frequency changes of the site to monitor the groundwater level and saturation of the subsoil, i.e., major vulnerability factors in case of strong earthquake shaking. Finally, such future long-term MHVSR campaigns would make it possible to record seismic events, a prerequisite for accurately estimating the site amplification and vulnerability of the Cusco built heritage.

Data and Resources

The supplemental material for this article is available on the Springer webpage.

References

Abbaszadeh Shahri A, Shan C, Zäll E, Larsson S (2021) Spatial distribution modeling of subsurface bedrock using a developed automated intelligence deep learning procedure: A case study in Sweden. J Rock Mech Geotech Eng 13:1300–1310. https://doi.org/10.1016/j.jrmge.2021.07.006

Albarello D, Lunedei E (2011) Structure of an ambient vibration wavefield in the frequency range of engineering interest ([0.5, 20] Hz): insights from numerical modelling. Surf Geophys 9:543–559. https://doi.org/10.3997/1873-0604.2011017

Alcántara Torres SN, Rucoba Hernández LE, Tayro Guerrero ARM, et al (2022) Determinación de periodos del suelo a partir de registros acelerográficos en la ciudad de Cusco. High School Graduate - Civil Engineering, PUCP

Alfaro C, Matos R, Beltrán-Caballero JA, Mar R (2015) El urbanismo Inka del Cusco. Nuevas Aportaciones. Arqueología y Arquitectura en la capital del Tawantinsuyu., Municipalidad del Cusco-NMAI Smithsonian Institution-Universitat Rovira i Virgili. Ricardo Mar, José Alejandro Beltrán-Caballero & Crayla Alfaro, Cusco-Washington-Tarragona

Anderson JG, Lee Y, Zeng Y, Day S (1996) Control of strong motion by the upper 30 meters. Bull Seismol Soc Am 86:1749–1759. https://doi.org/10.1785/BSSA0860061749

Antayhua Y, Garcia B, Rosell Guevara L, et al (2021) Caracterización magnetotelúrica de las fallas y sistema de fallas en el valle del Cusco, sur del Perú. Incasciences 1:64–77

Bard P-Y (1999) Microtremor measurements: A tool for site effect estimation? In: Irikura, Kudo, Okada, Sasatani (eds) Second International Symposium on the Effects of Surface Geology on seismic motion. Balkema Rotterdam, Yokohama, Japan, pp 1251–1279

Barrientos CW (2021) Peligro sísmico en la subcuenca del Cusco - 2019. PhD Dissertation, Universidad Andina del Cusco

Bauer BS (2018) Cuzco Antiguo: Tierra natal de los incas, 2nde édition actualisée. Centro de Estudios Regionales Andinos Bartolomé de las Casas, The Institute for New World Archaeology, Cusco

Beltrán-Caballero JA (2013) Agua y forma urbana en la América precolombina: el caso del Cusco como centro del poder inca. PhD Dissertation, Universidad Politécnica de Cataluña - Barcelona Tech (UPC)

Benavente C, Delgado Madera F, Taipe Maquerhua E, et al (2013) Neotectónica y Peligro Sísmico en la Región Cusco. INGEMMET, Lima

Benavente Velásquez R, Fernández Baca Vidal C, Gómez Noblega A (2004) Estudio del mapa de peligros de la ciudad de Cusco. PNUD-INDECI, Cusco

Bonnefoy-Claudet S, Cornou C, Bard P-Y, et al (2006) H/V ratio: a tool for site effects evaluation. Results from 1-D noise simulations. Geophys J Int 167:827–837. https://doi.org/10.1111/j.1365-246X.2006.03154.x

Bonnefoy-Claudet S, Kohler A, Cornou C, et al (2008) Effects of Love Waves on Microtremor H/V Ratio. Bull Seismol Soc Am 98:288–300. https://doi.org/10.1785/0120070063

Brando G, Cocco G, Mazzanti C, et al (2019) Structural Survey and Empirical Seismic Vulnerability Assessment of Dwellings in the Historical Centre of Cusco, Peru. Int J Archit Herit 1–29. https://doi.org/10.1080/15583058.2019.1685022

Brûlé S, Enoch S, Guenneau S (2020) Emergence of seismic metamaterials: Current state and future perspectives. Phys Lett A 384:126034. https://doi.org/10.1016/j.physleta.2019.126034

Brûlé S, Ungureanu B, Achaoui Y, et al (2017) Metamaterial-like transformed urbanism. Innov Infrastruct Solut 2:20. https://doi.org/10.1007/s41062-017-0063-x

Cabrera J (1988) Néotectonique et sismotectonique dans la Cordillère andine au niveau du changement de géométrie de la subduction: la région de Cuzco (Pérou). PhD Dissertation, Université Paris-Sud

Cabrera J, Sébrier M (1998) Surface Rupture Associated with a 5.3-mb Earthquake: The 5 April 1986 Cuzco Earthquake and Kinematics of the Chincheros-Qoricocha Faults of the High Andes, Peru. Bull Seismol Soc Am 88:242–255. https://doi.org/10.1785/BSSA0880010242

Cabrera J, Sébrier M, Mercier JL (1991) Plio-Quaternary geodynamic evolution of a segment of the Peruvian Andean Cordillera located above the change in the subduction geometry: the Cuzco region. Tectonophysics 190:331–362. https://doi.org/10.1016/0040-1951(91)90437-W

Calderon D, Aguilar Z, Lazares F, et al (2014) Development of a Seismic Microzoning Map for Lima City and Callao, Peru. J Disaster Res 9:939–945. https://doi.org/10.20965/jdr.2014.p0939

Candia-Gallegos MA, Sprenke KF, Perez JC (1993) Geotechnical Aspects on Seismic Risk Assessment in Cusco, Peru. In: Third International Conference on Case Histories in Geotechnical Engineering. St Louis, Missouri, pp 1763–1767

Carlier G, Lorand JP, Liégeois JP, et al (2005) Potassic-ultrapotassic mafic rocks delineate two lithospheric mantle blocks beneath the southern Peruvian Altiplano. Geology 33:601. https://doi.org/10.1130/G21643.1

Carlotto V, Cardénas J, Carlier G (2011) Geología del Cuadrángulo de Cusco 28-s - 1:50 000. INGEMMET, Lima

Castellaro S, Mulargia F (2009) The Effect of Velocity Inversions on H/V. Pure Appl Geophys 166:567–592. https://doi.org/10.1007/s00024-009-0474-5

CISMID, UNI (2013) Estudio de microzonificación sísmica y evaluación del riesgo en zonas ubicadas en el distrito del Cusco - Tomo I: Resumen ejecutivo. Centro Peruano-Japonés de Investigaciones Sísmicas y Mitigación de Desastres, Lima

Colombi A, Colquitt D, Roux P, et al (2016) A seismic metamaterial: The resonant metawedge. Sci Rep 6:27717. https://doi.org/10.1038/srep27717

Combey A, Audin L, Gandreau D, et al (2022) Reassessing the seismic hazard in the Cusco area, Peru: New contribution coming from an archaeoseismological survey on Inca remains. Quat Int 634:81–98. https://doi.org/10.1016/j.quaint.2022.07.003

D'Amico V, Picozzi M, Baliva F, Albarello D (2008) Ambient Noise Measurements for Preliminary Site-Effects Characterization in the Urban Area of Florence, Italy. Bull Seismol Soc Am 98:1373–1388. https://doi.org/10.1785/0120070231

Despotaki V, Silva V, Lagomarsino S, et al (2018) Evaluation of Seismic Risk on UNESCO Cultural Heritage sites in Europe. Int J Archit Herit 12:1231–1244. https://doi.org/10.1080/15583058.2018.1503374

Ericksen GE, Concha JF, Silgado E (1954) The Cusco, Peru, Earthquake of May 21, 1950. Bull Seismol Soc Am 44:97–112. https://doi.org/10.1785/BSSA04402A0097

Eurocode 8 (2005) Design of structures for earthquake resistance. Part 1: General rules, seismic actions and rules for buildings. British Standards Institution, London

Gallipoli MR, Mucciarelli M, Castro RR, et al (2004) Structure, soil–structure response and effects of damage based on observations of horizontal-to-vertical spectral ratios of microtremors. Soil Dyn Earthq Eng 24:487–495. https://doi.org/10.1016/j.soildyn.2003.11.009

García-Jerez A, Piña-Flores J, Sánchez-Sesma FJ, et al (2016) A computer code for forward calculation and inversion of the H/V spectral ratio under the diffuse field assumption. Comput Geosci 97:67–78. https://doi.org/10.1016/j.cageo.2016.06.016

Gregory HE (1916) A Geologic Reconnaissance of the Cuzco Valley, Peru. Am J Sci 4:1–100. https://doi.org/10.2475/ajs.s4-41.241.1

Guardia P, Tavera H (2015) Análisis de la microsismicidad asociada a las fallas de Tambomachay y Qoricocha, Cusco. Bol Soc Geológica Perú 110:201–204

Gueguen P, Bard P-Y, Chávez-García F (2002) Site-City Seismic Interaction in Mexico City-Like Environments: An Analytical Study. Bull Seismol Soc Am 92:794–811. https://doi.org/10.1785/0120000306

Gueguen P, Colombi A (2016) Experimental and Numerical Evidence of the Clustering Effect of Structures on Their Response during an Earthquake: A Case Study of Three Identical Towers in the City of Grenoble, France. Bull Seismol Soc Am 106:2855–2864. https://doi.org/10.1785/0120160057

Gupta RK, Agrawal M, Pal SK, Das MK (2021) Seismic site characterization and site response study of Nirsa (India). Nat Hazards 108:2033–2057. https://doi.org/10.1007/s11069-021-04767-w

INDECI-PNUD (2003) Estudio Geofísico de la ciudad del Cusco y zonas de expansión urbana para la elaboración de mapas del peligro. Universidad Nacional de San Agustín (UNSA), Arequipa

Irikura K, Kawanaka T (1980) Characteristics of Microtremors On Ground with Discontinuous Underground Structure. Bull Disaster Prev Res Inst 30:81–96

Khalili M, Mirzakurdeh AV (2019) Fault detection using microtremor data (HVSR-based approach) and electrical resistivity survey. J Rock Mech Geotech Eng 11:400–408. https://doi.org/10.1016/j.jrmge.2018.12.003

Konno K, Ohmachi T (1998) Ground-motion characteristics estimated from spectral ratio between horizontal and vertical components of microtremor. Bull Seismol Soc Am 88:228–241. https://doi.org/10.1785/BSSA0880010228

Kramer SL (1996) Geotechnical earthquake engineering. Prentice Hall, Upper Saddle River, NJ

Lachet C, Bard P-Y (1994) Numerical and Theoretical Investigations on the Possibilities and Limitations of Nakamura's Technique. J Phys Earth 42:377–397. https://doi.org/10.4294/jpe1952.42.377

Ladrón de Guevara O (1967) La Restauración del Ccoricancha y Templo de Santo Domingo. Rev Mus E Inst Arqueol 21:29–94

Lebrun B, Hatzfeld D, Bard PY (2001) Site Effect Study in Urban Area: Experimental Results in Grenoble (France). Pure Appl Geophys 158:2543–2557. https://doi.org/10.1007/PL00001185

Lombardo G, Rigano R (2006) Amplification of ground motion in fault and fracture zones: Observations from the Tremestieri fault, Mt. Etna (Italy). J Volcanol Geotherm Res 153:167–176. https://doi.org/10.1016/j.jvolgeores.2005.10.014

Lunedei E, Malischewsky P (2015) A Review and Some New Issues on the Theory of the H/V Technique for Ambient Vibrations. In: Ansal A (ed) Perspectives on European Earthquake Engineering and Seismology. Springer International Publishing, Cham, pp 371–394

Ma Y, Clayton RW (2014) The crust and uppermost mantle structure of Southern Peru from ambient noise and earthquake surface wave analysis. Earth Planet Sci Lett 395:61–70. https://doi.org/10.1016/j.epsl.2014.03.013

Mercier JL, Sebrier M, Lavenu A, et al (1992) Changes in the tectonic regime above a subduction zone of Andean Type: The Andes of Peru and Bolivia during the Pliocene-Pleistocene. J Geophys Res 97:11945–11982. https://doi.org/10.1029/90JB02473

Molnar S, Cassidy JF, Castellaro S, et al (2018) Application of Microtremor Horizontal-to-Vertical Spectral Ratio (MHVSR) Analysis for Site Characterization: State of the Art. Surv Geophys 39:613–631. https://doi.org/10.1007/s10712-018-9464-4

Molnar S, Sirohey A, Assaf J, et al (2022) A review of the microtremor horizontal-to-vertical spectral ratio (MHVSR) method. J Seismol 26:653–685. https://doi.org/10.1007/s10950-021-10062-9

Mucciarelli M, Gallipoli MR (2001) A critical review of 10 years of microtremor HVSR technique. Bolletino Geofis Teor Ed Appl 42:255–266

Mucciarelli M, Monachesi G, Gallipoli MR (1999) In Situ Measurements Of Site Effects And Building Dynamic Behaviour Related To Damage Observed During The 9/9/1998 Earthquake In Southern Italy. In: Proceedings of ERES99 Conference. Catania, Italy, pp 253–265

Nakamura Y (1989) A Method for Dynamic Characteristics Estimation of Subsurface Using Microtremor on the Ground Surface. Q Rep Railw Tech Res 30:25–33

Nakamura Y (2000) Clear Identification of Fundamental Idea of Nakamura's Technique and Its Applications. In: The 12th World Conference on Earthquake Engineering. Auckland, New Zealand

Nuñez MA (2021) Simulación de huaycos para la estimación de los niveles de peligro en el área de influencia de la quebrada Saphy, Cusco. Bachelor's Thesis, Universidad Nacional de San Agustín de Arequipa

Pacheco D, Mercerat ED, Courboulex F, et al (2022) Profiling the Quito basin (Ecuador) using seismic ambient noise. Geophys J Int 228:1419–1437. https://doi.org/10.1093/gji/ggab408

Palomino A, Benavente C, Rosell L, et al (2021) Caracterización Morfo-tectónica y paleo-sismológica del Sistema de Fallas Pachatusan - Cusco. INGEMMET, Lima

Parolai S, Picozzi M, Richwalski SM, Milkereit C (2005) Joint inversion of phase velocity dispersion and H/V ratio curves from seismic noise recordings using a genetic algorithm, considering higher modes. Geophys Res Lett 32:. https://doi.org/10.1029/2004GL021115

Pastén C, Sáez M, Ruiz S, et al (2015) Deep characterization of the Santiago Basin using HVSR and cross-correlation of ambient seismic noise. Eng Geol 201:57–66. https://doi.org/10.1016/j.enggeo.2015.12.021

Picozzi M, Parolai S, Albarello D (2005a) Statistical Analysis of Noise Horizontal-to-Vertical Spectral Ratios (HVSR). Bull Seismol Soc Am 95:1779–1786. https://doi.org/10.1785/0120040152

Picozzi M, Parolai S, Richwalski SM (2005b) Joint inversion of H/V ratios and dispersion curves from seismic noise: Estimating the S-wave velocity of bedrock. Geophys Res Lett 32:. https://doi.org/10.1029/2005GL022878

Pilz M, Parolai S, Leyton F, et al (2009) A comparison of site response techniques using earthquake data and ambient seismic noise analysis in the large urban areas of Santiago de Chile. Geophys J Int 178:713–728. https://doi.org/10.1111/j.1365-246X.2009.04195.x

Pischiutta M, Rovelli A, Salvini F, et al (2013) Directional resonance variations across the Pernicana Fault, Mt Etna, in relation to brittle deformation fields. Geophys J Int 193:986–996. https://doi.org/10.1093/gji/ggt031

Polo de Ondegardo J (1916) Informaciones acerca de la religión y gobierno de los incas. Imprenta y Librería Sanmartín & Co., Lima

Rong M, Fu L, Wang Z, et al (2017) On the Amplitude Discrepancy of HVSR and Site Amplification from Strong-Motion Observations. Bull Seismol Soc Am 107:2873–2884. https://doi.org/10.1785/0120170118

Rosell L, Benavente C, Zerathe S, et al (2023) Holocene Earthquakes on the Tambomachay Fault near Cusco, Central Andes. Tektonika 1:140–157. https://doi.org/10.55575/tektonika2023.1.2.27

Sébrier M, Mercier JL, Mégard F, et al (1985) Quaternary normal and reverse faulting and the state of stress in the central Andes of south Peru. Tectonics 4:739–780. https://doi.org/10.1029/TC004i007p00739

Seiner L (2016) Historia de los sismos en el Perú. Catálogo: Siglos XVIII-XIX, Fondo Editorial. Universidad de Lima, Lima

SESAME (2004) Guidelines for the Implementation of the H/V Spectral ratio technique of Ambient vibrations. Measurements, processing and interpretation

Silgado E, Concha JF, Ericksen GE (1952) El Terremoto del Cuzco del 21 de Mayo de 1950. Bol Inst Nac Investig Fom Min 2:27–46

Silgado E (1978) Historia de los sismos más notables ocurridos en el Perú (1513-1974). Instituto de Geología y Minería, Lima

Stanko D, Markušić S, Strelec S, Gazdek M (2017) HVSR analysis of seismic site effects and soil-structure resonance in Varaždin city (North Croatia). Soil Dyn Earthq Eng 92:666–677. https://doi.org/10.1016/j.soildyn.2016.10.022

Strollo A, Parolai S, Jackel K-H, et al (2008) Suitability of Short-Period Sensors for Retrieving Reliable H/V Peaks for Frequencies Less Than 1 Hz. Bull Seismol Soc Am 98:671–681. https://doi.org/10.1785/0120070055

Suárez G, Molnar P, Burchfiel BC (1983) Seismicity, fault plane solutions, depth of faulting, and active tectonics of the Andes of Peru, Ecuador, and southern Colombia. J Geophys Res Solid Earth 88:10403–10428. https://doi.org/10.1029/JB088iB12p10403

Tarabusi G, Caputo R (2017) The use of HVSR measurements for investigating buried tectonic structures: the Mirandola anticline, Northern Italy, as a case study. Int J Earth Sci 106:341–353. https://doi.org/10.1007/s00531-016-1322-3

Tibaldi A, Bonali FL, Pasquaré Mariotto F, et al (2024) Structural expression of the frontal thrust of an active fold-and-thrust belt: The Holocene 123-km-long Kur fault, Greater Caucasus, Azerbaijan. J Struct Geol 180:105085. https://doi.org/10.1016/j.jsg.2024.105085

Villanueva H (1970) Documentos sobre el terremoto de 1650. Rev Arch Histórico Cuzco 203–220

Vranich A, Berquist S, Hardy T (2014) Prehistoric Urban Archaeology in the Americas: A View from Cusco, Peru. Learn Past Prep Future Annual Review of the Cotsen Institute of Archaeology at UCLA:57–67

Wathelet M, Chatelain J-L, Cornou C, et al (2020) Geopsy: A User-Friendly Open-Source Tool Set for Ambient Vibration Processing. Seismol Res Lett 91:1878–1889. https://doi.org/10.1785/0220190360

Wimpenny S, Benavente C, Copley A, et al (2020) Observations and dynamical implications of active normal faulting in South Peru. Geophys J Int 222:27–53. https://doi.org/10.1093/gji/ggaa144

Wright KR (2006) Tipon. Water Engineering Masterpiece of the Inca Empire, American Society of Civil Engineers Press. Reston, Virginia

Xu R, Wang L (2021) The horizontal-to-vertical spectral ratio and its applications. EURASIP J Adv Signal Process 2021:75. https://doi.org/10.1186/s13634-021-00765-z

Zavala N, Clemente-Chávez A, Figueroa-Soto Á, et al (2021) Application of horizontal to Vertical Spectral Ratio microtremor technique in the analysis of site effects and structural response of buildings in Querétaro city, Mexico. J South Am Earth Sci 108:103211. https://doi.org/10.1016/j.jsames.2021.103211

Statements and Declarations

Acknowledgements/Funding

This work would not have been possible without the collaboration of Architect Eliluz Palomino of the Gerencia del Centro Histórico de Cusco and Archaeologist Yeny Baca of the Dirección Desconcentrada del Ministerio de Cultura de Cusco. We also thank Fabrizio Delgado, Cristhian Baca, Julio Rojas, Enoch Aguirre for their precious assistance and expertise during the field campaigns. Finally, the authors would like to show their gratitude to the two anonymous reviewers and the editor whose suggestions helped improve and clarify this article. This work has been supported by the French government, through the UCA^{JEDI} Investments in the Future project managed by the National Research Agency (ANR) with the reference number ANR-15-IDEX-01. It was also supported by the Peruvian Ministry of Energy and Mines, through the Institute of Geology, Mining and Metallurgy (Geological Survey) and the Neotectonics project of the Department of Environmental Geology and Geological Risk. The project has received, as well, financial support from the UMR 7329 Geoazur Laboratory.

Competing interests

The authors have no relevant financial or non-financial interests to disclose.

Author Contributions:

Conceptualization: *A. Combey, E.D. Mercerat, C.L. Benavente*; Methodology: *A. Combey, E.D. Mercerat, J.E. Díaz, F.P. Perez*; Formal analysis and investigation: *A. Combey, E.D. Mercerat, J.E. Díaz;* Writing - original draft preparation: *A. Combey*; Funding acquisition: *A. Combey, E.D. Mercerat, C.L. Benavente*; Resources: *B. García, A.R. Palomino, C.J. Guevara*; Supervision: *A. Combey, E.D. Mercerat, C.L. Benavente*.